

Statistical Properties of Eigen-Modes and Instantaneous Mutual Information in MIMO Time-Varying Rayleigh Channels

Shuangquan Wang, *Student Member, IEEE*, and Ali Abdi, *Member, IEEE*

Abstract

In this paper, we study two important metrics in multiple-input multiple-output (MIMO) time-varying Rayleigh flat fading channels. One is the eigen-mode, and the other is the instantaneous mutual information (IMI). Their second-order statistics, such as the correlation coefficient, level crossing rate (LCR), and average fade/outage duration, are investigated, assuming a general *nonisotropic* scattering environment. Exact closed-form expressions are derived and Monte Carlo simulations are provided to verify the accuracy of the analytical results. For the eigen-modes, we found they tend to be spatio-temporally uncorrelated in large MIMO systems. For the IMI, the results show that its correlation coefficient can be well approximated by the squared amplitude of the correlation coefficient of the channel, under certain conditions. Moreover, we also found the LCR of IMI is much more sensitive to the scattering environment than that of each eigen-mode.

Index Terms

Eigen-Modes, Instantaneous Mutual Information, Autocorrelation Function, Correlation Coefficient, Level Crossing Rate, Average Fade/Outage Duration, and Multiple-Input Multiple-Output (MIMO).

I. INTRODUCTION

The utilization of antenna arrays at the base station (BS) and the mobile station (MS) in a wireless communication system increases the capacity linearly with $\min(N_T, N_R)$, under certain conditions, where N_T and N_R are numbers of transmit and receive antenna elements, respectively, provided that the environment is sufficiently rich in multi-path components [1][2]. This is due to the fact that a multiple-input multiple-output (MIMO) channel can be decomposed to several parallel single-input single-output (SISO) channels, called *eigen-channels* or *eigen-modes*¹, via singular value decomposition (SVD) [2]–[9].

This paper was presented in part at the *40th Ann. Conf. Info. Sci. Sys.*, Princeton, NJ, 2006.

The authors are with the Center for Wireless Communications and Signal Processing Research (CWCSRP), Department of Electrical and Computer Engineering, New Jersey Institute of Technology, Newark, NJ 07102 USA (e-mail:{sw27, ali.abdi}@njit.edu).

¹We use the two terms interchangeably in this paper.

For a SISO channel, or any subchannel² of a MIMO system, there are numerous studies on key second-order statistics such as correlation, level crossing rate (LCR), and average fade duration (AFD) [10]–[14]. However, to the best of our knowledge, no such study on the *eigen*-channels of a MIMO system is reported in the literature, possibly due to the lack of knowledge regarding the joint probability density function (PDF) of *eigen*-channels.

Regarding another important quantity, the *instantaneous mutual information* (IMI), only some first-order statistics such as the mean, variance, outage probability and PDF are studied [9][15]–[18]. Clearly, those statistics do not show the dynamic temporal behavior, such as correlations, LCR and average outage durations (AOD) of the IMI in time-varying fading channels. It is known that IMI can be feedbacked to the rate scheduler in multi-user communication environments, to increase the system throughput [16], where only the perfect feedback is considered. However, it is hard to obtain perfect feedback in practice due to the time-varying nature of the channel, which makes the feedbacked IMI outdated. In this case, the temporal correlation of IMI can be used to analyze the scheduling performance with outdated IMI feedbacks. Furthermore, one can improve the rate scheduling algorithm by exploring the temporal correlation of IMI.

Several second-order statistics such as the correlation coefficient, LCR and AOD of IMI in single-input single-output (SISO) systems are reported in [19] and [20]. For MRC-like MIMO systems, they are investigated in [20]. However, there are a limited number of results for a general MIMO channel. In [21], some simulation results regarding the correlation coefficient, LCR and AOD are reported, without analytical derivations. In [22], lower and upper bounds, as well as some approximations for the correlation coefficient of IMI are derived, without exact results at high SNR. A large gap between the lower and upper bounds and large approximation errors are observed in [22, Figs. 2, 5].

In this paper, we extend the results of [20] to the general MIMO case, using the joint PDF of the eigenvalues [23]. Specifically, a number of second-order statistics such as the autocorrelation function (ACF), the correlation coefficient, LCR and AFD/AOD³ of the *eigen*-channels and the IMI are studied in MIMO time-varying Rayleigh flat fading channels. We assume all the subchannels are spatially independent and identically distributed (i.i.d.), with the same temporal correlation coefficient, considering general *nonisotropic* scattering propagation environments. Closed-form expressions are derived, and Monte Carlo simulations are provided to verify the accuracy of our closed-form expressions. The simulation and analytical results show that the eigen-modes tend to be spatio-temporally uncorrelated in large MIMO systems, and the correlation coefficient of the IMI can be well approximated by the squared amplitude of the correlation coefficient of the channel if $|N_T - N_R|$ is much larger than $\min(N_T, N_R)$. In addition, we also observed that the LCR of IMI is much more sensitive to the scattering environment than that of each eigen-mode.

The rest of this paper is organized as follows. Section II introduces the channel model, as well as the angle-of-arrival (AoA) model. *Eigen*-channels of a MIMO system are discussed in Section III, where Subsection III-A

²In this paper, each subchannel represents the radio link between each transmit/receive pair of antennas.

³Note that AFD is used for eigen-channels, whereas AOD is used for MIMO IMI.

is devoted to the derivation of the normalized ACF (NACF) and the correlation coefficient of *eigen*-channels of a MIMO system, whereas Subsection III-B focuses on the LCR and AFD of the *eigen*-channels. The MIMO IMI is investigated in Section IV, in which Subsection IV-A addresses the NACF and the correlation coefficient of the MIMO IMI as well as their low- and high-SNR approximations, whereas Subsection IV-B studies the LCR and AOD of the MIMO IMI using the well-known Gaussian approximation. Numerical results and discussions are presented in Section V, and concluding remarks are given in Section VI.

Notation: \cdot^\dagger is reserved for matrix Hermitian, \cdot^* for complex conjugate, j for $\sqrt{-1}$, $\mathbb{E}[\cdot]$ for mathematical expectation, \mathbf{I}_m for the $m \times m$ identity matrix, $\|\cdot\|_F$ for the Frobenius norm, $\Re[\cdot]$ and $\Im[\cdot]$ for the real and imaginary parts of a complex number, respectively, and $f^2(x)$ for $[f(x)]^2$. Finally, $t \in [m, n]$ implies that t , m and n are integers such that $m \leq t \leq n$ with $m \leq n$.

II. CHANNEL MODEL

In this paper, an $N_R \times N_T$ MIMO time-varying Rayleigh flat fading channel is considered. Similar to [15], we consider a piecewise constant approximation for the continuous-time MIMO fading channel matrix coefficient $\mathbf{H}(t)$, represented by $\{\mathbf{H}(lT_s)\}_{l=1}^L$, where T_s is the symbol duration and L is the number of samples. In the sequel, we drop T_s to simplify the notation. In the l^{th} symbol duration, the matrix of the channel coefficients is given by

$$\mathbf{H}(l) = \begin{bmatrix} h_{1,1}(l) & \cdots & h_{1,N_T}(l) \\ \vdots & \ddots & \vdots \\ h_{N_R,1}(l) & \cdots & h_{N_R,N_T}(l) \end{bmatrix}, l \in [1, L]. \quad (1)$$

We assume all the $N_T N_R$ subchannels $\{h_{n_r, n_t}(l), l \in [1, L]\}_{(n_r=1, n_t=1)}^{(N_R, N_T)}$ are i.i.d., with the same temporal correlation coefficient, i.e.,

$$\mathbb{E}[h_{mn}(l)h_{pq}^*(l-i)] = \delta_{m,p}\delta_{n,q}\rho_h(i), \quad (2)$$

where the Kronecker delta $\delta_{m,p}$ is 1 or 0 when $m = p$ or $m \neq p$, respectively, and $\rho_h(i)$ is defined and derived at the end of this section, eq. (4).

In flat Rayleigh fading channels, each $h_{n_r, n_t}(l), l \in [1, L]$, is a zero-mean complex Gaussian random process. In the l^{th} interval, $h_{n_r, n_t}(l)$ can be represented as [13]

$$\begin{aligned} h_{n_r, n_t}(l) &= h_{n_r, n_t}^I(l) + jh_{n_r, n_t}^Q(l), \\ &= \alpha_{n_r, n_t}(l) \exp[-j\Phi_{n_r, n_t}(l)], \end{aligned} \quad (3)$$

where the zero-mean real Gaussian random processes $h_{n_r, n_t}^I(l)$ and $h_{n_r, n_t}^Q(l)$ are the real and imaginary parts of $h_{n_r, n_t}(l)$, respectively. $\alpha_{n_r, n_t}(l)$ is the envelope of $h_{n_r, n_t}(l)$ and $\Phi_{n_r, n_t}(l)$ is the phase of $h_{n_r, n_t}(l)$. For each l , $\alpha_{n_r, n_t}(l)$ has a Rayleigh distribution and $\Phi_{n_r, n_t}(l)$ is distributed uniformly over $[-\pi, \pi)$. Without loss of generality, we assume each subchannel has unit power, i.e., $\mathbb{E}[\alpha_{n_r, n_t}^2(l)] = 1$.

Using empirically-verified [13] multiple von Mises PDF's [19, (4)] for the AoA at the receiver in *nonisotropic* scattering environments, shown as Fig. 1 of [19], the channel correlation coefficient of $h_{n_r, n_t}(l), \forall n_r, n_t$, is given

by [19, (7)]

$$\begin{aligned}\rho_h(i) &= \mathbb{E}[h_{n_r, n_t}(l)h_{n_r, n_t}^*(l-i)], \\ &= \sum_{n=1}^N P_n \frac{I_0\left(\sqrt{\kappa_n^2 - 4\pi^2 f_D^2 i^2 T_s^2 + j4\pi\kappa_n f_D i T_s} \cos\theta_n\right)}{I_0(\kappa_n)},\end{aligned}\quad (4)$$

where $I_k(z) = \frac{1}{\pi} \int_0^\pi e^{z \cos w} \cos(kw) dw$ is the k^{th} order modified Bessel function of the first kind, θ_n is the mean AoA of the n^{th} cluster of scatterers, κ_n controls the width of the n^{th} cluster of scatterers, P_n represents the contribution of the n^{th} cluster of scatterers such that $\sum_{n=1}^K P_n = 1, 0 < P_n \leq 1$, K is the number of clusters of scatterers, and f_D is the maximum Doppler frequency. When $\kappa_n = 0, \forall n$, which corresponds to *isotropic* scattering, (4) reduces to $\rho_h(i) = I_0(j2\pi f_D i T_s) = J_0(2\pi f_D i T_s)$, which is the Clarke's correlation model.

III. EIGEN-CHANNELS IN MIMO SYSTEMS

We set $M = \min(N_T, N_R)$ and $N = \max(N_T, N_R)$. Based on singular value decomposition (SVD) [2]–[9], $\mathbf{H}(l)$ in (1) can be diagonalized in the following form

$$\mathbf{H}(l) = \mathbf{U}(l)\mathbf{S}(l)\mathbf{V}^\dagger(l), \quad (5)$$

where $\mathbf{V}(l)$, whose dimension is $N_T \times M$, satisfies $\mathbf{V}^\dagger(l)\mathbf{V}(l) = \mathbf{I}_M$, $\mathbf{U}(l)$, which is $N_R \times M$, satisfies $\mathbf{U}^\dagger(l)\mathbf{U}(l) = \mathbf{I}_M$, and $\mathbf{S}(l)$ is a diagonal matrix, given by $\mathbf{S}(l) = \text{diag}[s_1(l), \dots, s_M(l)]$, in which $s_m(l)$, $m \in [1, M]$ is the m^{th} non-zero singular value of $\mathbf{H}(l)$.

We define $\lambda_m(l) = s_m^2(l)$, $\forall m$. Therefore $\lambda_m(l)$ is the m^{th} non-zero eigenvalue of $\mathbf{H}(l)\mathbf{H}^\dagger(l)$. We further consider $\{\lambda_m(l)\}_{m=1}^M$ as unordered non-zero eigenvalues of $\mathbf{H}(l)\mathbf{H}^\dagger(l)$. Therefore, the MIMO channel $\mathbf{H}(l)$ is decomposed to M identically distributed *eigen-channels*, $\{\lambda_m(l), l \in [1, L]\}_{m=1}^M$, by SVD, as shown in Fig. 1. For $M = 1$, there is only one *eigen-channel*, which corresponds to the maximal ratio transmitter (MRT) if $N_R = 1$, or the maximal ratio combiner (MRC) if $N_T = 1$. In each case, we have N i.i.d complex Gaussian branches.

Since all the *eigen-channels* have identical statistics, we only study one of them and denote it as $\lambda(l), l \in [1, L]$. To simplify the notation, we use X and Y to denote $\lambda(l)$ and $\lambda(l-i)$, respectively. The joint PDF of X and Y is given in (6) of [23],

$$\begin{aligned}p(x, y) &= \frac{(xy)^{\frac{\nu}{2}} e^{-\frac{x+y}{1-\varrho_i^2}} I_\nu\left(\frac{2\varrho_i \sqrt{xy}}{1-\varrho_i^2}\right)}{M^2(1-\varrho_i^2)\varrho_i^\nu} \sum_{k=0}^{M-1} \frac{k! L_k^\nu(x) L_k^\nu(y)}{(k+\nu)! \varrho_i^{2k}} + \frac{(xy)^\nu e^{-(x+y)}}{M^2} \sum_{0 \leq k < l}^{M-1} \left\{ \frac{k! l!}{(k+\nu)!(l+\nu)!} \right. \\ &\quad \left. \times \left\{ [L_k^\nu(x) L_l^\nu(y)]^2 + [L_l^\nu(x) L_k^\nu(y)]^2 - \left[\varrho_i^{2(l-k)} + \varrho_i^{2(k-l)} \right] L_k^\nu(x) L_l^\nu(x) L_k^\nu(y) L_l^\nu(y) \right\} \right\},\end{aligned}\quad (6)$$

where $L_n^\alpha(x) = \frac{1}{n!} e^x x^{-\alpha} \frac{d^n}{dx^n} (e^{-x} x^{n+\alpha})$ is the associated Laguerre polynomial of order n [24, pp. 1061, 8.970.1], $\nu = N - M$, and $\varrho_i = |\rho_h(i)|$, where $\rho_h(i)$ is given in (4). The joint PDF in (6) is very general and includes many existing PDF's as special cases [23].

- By integration over y , (6) reduces to the marginal PDF

$$p(x) = \frac{1}{M} \sum_{m=0}^{M-1} \frac{m!}{(m+\nu)!} [L_m^\nu(x)]^2 x^\nu e^{-x}, \quad (7)$$

which is the same as the PDF presented in [2]. When $M = 1$, (7) further reduces to

$$p(x) = \frac{1}{(N-1)!} x^{N-1} e^{-x}, \quad (8)$$

which is the χ^2 distribution with $2N$ degrees of freedom [25, (2.32)], used for characterizing the PDF of outputs of MRT or MRC [26].

- With $M = 1$, (6) reduces to

$$p(x, y) = \frac{(xy)^{\frac{N-1}{2}} \exp\left(-\frac{x+y}{1-\rho_i^2}\right) I_{N-1}\left(\frac{2\rho_i\sqrt{xy}}{1-\rho_i^2}\right)}{(N-1)! (1-\rho_i^2) \rho_i^{N-1}}, \quad (9)$$

which is the joint PDF of outputs of MRT or MRC at the l^{th} and $(l-i)^{\text{th}}$ symbol durations [27]. It includes (3.14) of [25] as a special case⁴. Furthermore, when $N = 1$, i.e., a SISO channel, (9) simplifies to

$$p(x, y) = \frac{1}{1-\rho_i^2} \exp\left(-\frac{x+y}{1-\rho_i^2}\right) I_0\left(\frac{2\rho_i\sqrt{xy}}{1-\rho_i^2}\right), \quad (10)$$

which is identical to (8-103) [28, pp. 163], after a one-to-one nonlinear mapping.

In the following subsections, we study the normalized correlation and correlation coefficient of any two eigen-channels, defined by, respectively,

$$\tilde{r}_{m,n}(i) = \frac{\mathbb{E}[\lambda_m(l)\lambda_n(l-i)]}{\sqrt{\mathbb{E}[\lambda_m^2(l)]}\sqrt{\mathbb{E}[\lambda_n^2(l-i)]}}, \quad (11)$$

and

$$\rho_{m,n}(i) = \frac{\mathbb{E}[\lambda_m(l)\lambda_n(l-i)] - \mathbb{E}[\lambda_m(l)]\mathbb{E}[\lambda_n(l-i)]}{\sqrt{\mathbb{E}[\lambda_m^2(l)] - \{\mathbb{E}[\lambda_m(l)]\}^2} \sqrt{\mathbb{E}[\lambda_n^2(l-i)] - \{\mathbb{E}[\lambda_n(l-i)]\}^2}}, \quad (12)$$

A. Normalized Correlation and Correlation Coefficient of Eigen-Channels

To derive the normalized correlation and correlation coefficient between any two eigen-channels, we need the following lemmas.

Lemma 1: The first and second moments of the m^{th} eigen-channel are respectively given by

$$\mathbb{E}[\lambda_m(l)] = N, \quad (13)$$

$$\mathbb{E}[\lambda_m^2(l)] = N(N+M). \quad (14)$$

Proof: See Appendix I. □

Lemma 2: The autocorrelation of the m^{th} eigen-channel, defined as $r_{m,m}(i) = \mathbb{E}[\lambda_m(l)\lambda_m(l-i)]$, is given by

$$r_{m,m}(i) = N^2 + \frac{N\rho_i^2}{M}, \quad i \neq 0. \quad (15)$$

Proof: See Appendix II. □

Lemma 3: The cross-correlation between the m^{th} and n^{th} eigen-channels, defined as $r_{m,n}(i) = \mathbb{E}[\lambda_m(l)\lambda_n(l-i)]$, is given by

$$r_{m,n}(i) = \begin{cases} N^2 - N, & i = 0, \\ N^2 + \frac{N\rho_i^2}{M}, & i \neq 0, \end{cases} \quad n \neq m. \quad (16)$$

⁴Eq. (3.14) in [25] is developed for real uncorrelated Gaussian random variables.

Proof: See Appendix III. \square

Based on Lemmas 1-3, we obtain the closed-form expressions for (11) and (12), which are given in the following theorem.

Theorem 1: The normalized cross-correlation and the correlation coefficient between m^{th} and n^{th} eigen-channels, defined in (11) and (12), are respectively given by

$$\tilde{r}_{m,n}(i) = \begin{cases} \frac{M-(M+1)(1-\delta_{m,n})}{N+M}, & i = 0, \\ \frac{MN+\varrho_i^2}{MN+M^2}, & i \neq 0, \end{cases} \quad (17)$$

and

$$\rho_{m,n}(i) = \begin{cases} 1 - \frac{M+1}{M} (1 - \delta_{m,n}), & i = 0, \\ \frac{\varrho_i^2}{M^2}, & i \neq 0. \end{cases} \quad (18)$$

Proof: From Lemma 1, it is straightforward to see that the eigen-channel is stationary in the wide sense. Moreover, all the eigen-channels have the same statistics, therefore we have $\mathbb{E}[\lambda_n(l-i)] = \mathbb{E}[\lambda_m(l)]$ and $\mathbb{E}[\lambda_n^2(l-i)] = \mathbb{E}[\lambda_m^2(l)]$, $\forall m, n \in [1, M]$ and $\forall l, i$. By plugging (14)-(15) into (11), we obtain (17). Finally, substitution of (13)-(15) into (12) results in (18). \square

From (17) and (18), we have the following interesting observations.

- If M is greater than 1, the normalized correlation and the correlation coefficient are not continuous at $i = 0$, as $\tilde{r}_{m,n}(1)$ and $\rho_{m,n}(1)$ do not converge to $\tilde{r}_{m,n}(0) = \rho_{m,n}(0) = 1$ as $T_s \rightarrow 0$, $\forall m, n$.
- If M is large, all the M eigen-channels tend to be spatio-temporally uncorrelated, due to

$$\lim_{M \rightarrow \infty} \rho_{m,n}(i) = \delta_{m,n} \delta_{i,0}. \quad (19)$$

As an example, with isotropic scattering, (17) and (18), respectively, reduce to

$$\tilde{r}_{m,n}(i) = \begin{cases} \frac{M-(M+1)(1-\delta_{m,n})}{N+M}, & i = 0, \\ \frac{MN+J_0^2(2\pi f_D i T_s)}{MN+M^2}, & i \neq 0, \end{cases} \quad (20)$$

and

$$\rho_{m,n}(i) = \begin{cases} 1 - \frac{M+1}{M} (1 - \delta_{m,n}), & i = 0, \\ \frac{J_0^2(2\pi f_D i T_s)}{M^2}, & i \neq 0, \end{cases} \quad (21)$$

B. LCR and AFD of an Eigen-Channel

In this subsection, we calculate the LCR and AFD of an eigen-channel at a given level. To simplify the notation, the eigen-channel index m is dropped in this subsection, as the derived LCR and AFD results hold for any eigen-channel.

1) *LCR of an Eigen-Channel:* Similar to the calculation of zero crossing rate in discrete time [29, Ch. 4], we define the binary sequence $\{Z_l\}_{l=1}^L$, based on the eigen-channel samples $\{\lambda(l)\}_{l=1}^L$, as

$$Z_l = \begin{cases} 1, & \text{if } \lambda(l) \geq \lambda_{\text{th}}, \\ 0, & \text{if } \lambda(l) < \lambda_{\text{th}}, \end{cases} \quad (22)$$

where λ_{th} is a fixed threshold. The number of crossings of $\{\lambda(l)\}_{l=1}^L$ with λ_{th} , within the time interval $T_s \leq t \leq LT_s$, denoted by $D_{\lambda_{\text{th}}}$, can be defined in terms of $\{Z_l\}_{l=1}^L$ [29, (4.1)]

$$D_{\lambda_{\text{th}}} = \sum_{l=2}^L (Z_l - Z_{l-1})^2, \quad (23)$$

which includes both up- and down-crossings.

After some simple manipulations, the expected crossing rate at the level λ_{th} can be written as

$$\frac{\mathbb{E}[D_{\lambda_{\text{th}}}]}{(L-1)T_s} = \frac{2P_r\{Z_l = 1\} - 2P_r\{Z_l = 1, Z_{l-1} = 1\}}{T_s}, \quad (24)$$

where $P_r\{\cdot\}$ is the probability of an event. Therefore, the expected down crossing rate at λ_{th} , denoted by $N_{\lambda}(\lambda_{\text{th}})$, is half of (24), given by

$$N_{\lambda}(\lambda_{\text{th}}) = \frac{\phi_{\lambda}(\lambda_{\text{th}}) - \varphi_{\lambda}(\lambda_{\text{th}})}{T_s}, \quad (25)$$

where $\phi_{\lambda}(\lambda_{\text{th}}) = P_r\{Z_l = 1\}$ and $\varphi_{\lambda}(\lambda_{\text{th}}) = P_r\{Z_l = 1, Z_{l-1} = 1\}$. Analytical expressions for $\phi_{\lambda}(\lambda_{\text{th}})$ and $\varphi_{\lambda}(\lambda_{\text{th}})$ are stated in the following theorem.

Theorem 2: For a given threshold λ_{th} , $\phi_{\lambda}(\lambda_{\text{th}})$ and $\varphi_{\lambda}(\lambda_{\text{th}})$ are, respectively, given by

$$\phi_{\lambda}(\lambda_{\text{th}}) = \frac{1}{M} \sum_{m=0}^{M-1} \sum_{p=0}^m \sum_{q=0}^m \frac{m! \binom{m+\nu}{m-p} \binom{m+\nu}{m-q} \Gamma(p+q+\nu+1, \lambda_{\text{th}})}{(m+\nu)! p! q! (-1)^{p+q}}, \quad (26)$$

and

$$\varphi_{\lambda}(\lambda_{\text{th}}) = \phi_{\lambda}^2(\lambda_{\text{th}}) + \frac{1}{M^2} \sum_{j=M}^{\infty} \sum_{k=0}^{M-1} \frac{j! k! \varrho_1^{2(j-k)}}{(j+\nu)! (k+\nu)!} \left[\sum_{p=0}^j \sum_{q=0}^k \frac{\binom{j+\nu}{j-p} \binom{k+\nu}{k-q}}{p! q! (-1)^{p+q}} \Gamma(p+q+\nu+1, \lambda_{\text{th}}) \right]^2, \quad (27)$$

where $\Gamma(a, z) = \int_z^{\infty} t^{a-1} e^{-t} dt$ [24, pp. 949, 8.350.2] is the upper incomplete gamma function, $\binom{n}{k}$ is the binomial coefficient, given by $\frac{n!}{k!(n-k)!}$, and $\varrho_1 = |\rho_h(1)|$, defined before, i.e.,

$$\varrho_1 = \left| \sum_{n=1}^N P_n \frac{I_0(\sqrt{\kappa_n^2 - 4\pi^2 f_D^2 T_s^2 + j4\pi\kappa_n f_D T_s \cos \theta_n})}{I_0(\kappa_n)} \right|. \quad (28)$$

Proof: $L_n^{\nu}(x)$ is a polynomial of order n , and can be represented as [24, pp. 1061, 8.970.1]

$$L_n^{\nu}(x) = \sum_{k=0}^n \binom{n+\nu}{n-k} \frac{(-x)^k}{k!}. \quad (29)$$

By plugging (29) into (7), the univariate PDF of an eigen-channel, and integrating over x from λ_{th} to ∞ , we obtain (26). Similarly, substitution of (29) into (64), the bivariate PDF of an eigen-channel, and integration over x from λ_{th} to ∞ results in (27). \square

By plugging (26) and (27) into (25), we obtain the expected crossing rate at the level λ_{th} .

2) *AFD of an Eigen-Channel:* The cumulative distribution function (CDF) of $\lambda(l)$, $\forall l$, is obtained as

$$F_{\lambda}(\lambda_{\text{th}}) = P_r\{X \leq \lambda_{\text{th}}\} = 1 - \phi_{\lambda}(\lambda_{\text{th}}), \quad (30)$$

where $\phi_{\lambda}(\lambda_{\text{th}})$ is given in (26).

The AFD of the *eigen-channel* $\{\lambda(l)\}_{l=1}^L$ is therefore given by

$$\bar{t}_{\lambda}(\lambda_{\text{th}}) = \frac{F_{\lambda}(\lambda_{\text{th}})}{N_{\lambda}(\lambda_{\text{th}})} = \frac{[1 - \phi_{\lambda}(\lambda_{\text{th}})]T_s}{\phi_{\lambda}(\lambda_{\text{th}}) - \varphi_{\lambda}(\lambda_{\text{th}})}, \quad (31)$$

where $\phi_\lambda(\lambda_{\text{th}})$ and $\varphi_\lambda(\lambda_{\text{th}})$ are given in (26) and (27), respectively.

IV. MIMO IMI

In this section, the NACF, the correlation coefficient, LCR and AOD of IMI in a MIMO system are investigated in detail. In the presence of the additive white Gaussian noise, if perfect channel state information $\{\mathbf{H}(l)\}_{l=1}^L$, is available at the receiver only, the ergodic channel capacity is given by [2][9]

$$C = \mathbb{E} \left[\ln \det \left(\mathbf{I}_{N_R} + \frac{\eta}{N_T} \mathbf{H}_l \mathbf{H}_l^\dagger \right) \right], \quad (32)$$

in nats/s/Hz, where η is the average SNR at each receive antenna, and \mathbf{H}_l denotes $\mathbf{H}(l)$.

In the above equation, at any given time index l , $\ln \det \left(\mathbf{I}_{N_R} + \frac{\eta}{N_T} \mathbf{H}_l \mathbf{H}_l^\dagger \right)$ is a random variable as it depends on the random channel matrix \mathbf{H}_l . Therefore

$$\mathcal{I}_l = \ln \det \left(\mathbf{I}_{N_R} + \frac{\eta}{N_T} \mathbf{H}_l \mathbf{H}_l^\dagger \right), \quad l = 1, 2, \dots, \quad (33)$$

is a discrete-time random process with the ergodic capacity as its mean.

By plugging (5) into (33), we can express the IMI in terms of M eigenvalues as

$$\mathcal{I}_l = \sum_{m=1}^M \ln \left(1 + \frac{\eta}{N_T} \lambda_m(l) \right), \quad l = 1, 2, \dots. \quad (34)$$

A. NACF and Correlation Coefficient of MIMO IMI

In this subsection, we derive exact closed-form expression for the NACF and the correlation coefficient of MIMO IMI, and their approximations at low- and high-SNR regimes, using the following lemmas.

Lemma 4: The mean and second moment of \mathcal{I}_l are respectively given by (35) and (36)

$$\mathbb{E}[\mathcal{I}_l] = \sum_{m=0}^{M-1} \sum_{p=0}^m \sum_{q=0}^m \frac{m! \binom{m+\nu}{m-p} \binom{m+\nu}{m-q}}{(m+\nu)! p! q! (-1)^{p+q}} G_{2,3}^{3,1} \left(\frac{N_T}{\eta} \middle| \begin{matrix} 0, 1 \\ 0, 0, p+q+\nu+1 \end{matrix} \right), \quad (35)$$

$$\begin{aligned} \mathbb{E}[\mathcal{I}_l^2] &= 2e^{\frac{N_T}{\eta}} \sum_{m=0}^{M-1} \sum_{p=0}^m \sum_{q=0}^m \sum_{j=0}^{p+q+\nu} \frac{(-1)^{\nu-j} m! \binom{m+\nu}{m-p} \binom{m+\nu}{m-q} \binom{p+q+\nu}{j}}{\left(\frac{\eta}{N_T}\right)^{p+q+\nu+1} (m+\nu)! p! q!} G_{3,4}^{4,0} \left(\frac{N_T}{\eta} \middle| \begin{matrix} -j, -j, -j \\ 0, -j-1, -j-1, -j-1 \end{matrix} \right) \\ &\quad - \sum_{j=0}^{M-1} \sum_{k=0}^{M-1} \frac{j! k!}{(j+\nu)! (k+\nu)!} \left[\sum_{p=0}^j \sum_{q=0}^k \frac{\binom{j+\nu}{j-p} \binom{k+\nu}{k-q}}{p! q! (-1)^{p+q}} G_{2,3}^{3,1} \left(\frac{N_T}{\eta} \middle| \begin{matrix} 0, 1 \\ 0, 0, p+q+\nu+1 \end{matrix} \right) \right]^2 + \{\mathbb{E}[\mathcal{I}_l]\}^2, \quad (36) \end{aligned}$$

where G is Meijer's G function [24, pp. 1096, 9.301].

Proof: See Appendix IV. □

Lemma 5: The ACF of MIMO IMI, defined as $r_{\mathcal{I}}(i) = \mathbb{E}[\mathcal{I}_l \mathcal{I}_{l-i}]$, is shown to be

$$r_{\mathcal{I}}(i) = \{\mathbb{E}[\mathcal{I}_l]\}^2 + \sum_{j=M}^{\infty} \sum_{k=0}^{M-1} \frac{j! k! \varrho_i^{2(j-k)}}{(j+\nu)! (k+\nu)!} \left[\sum_{p=0}^j \sum_{q=0}^k \frac{\binom{j+\nu}{j-p} \binom{k+\nu}{k-q}}{p! q! (-1)^{p+q}} G_{2,3}^{3,1} \left(\frac{N_T}{\eta} \middle| \begin{matrix} 0, 1 \\ 0, 0, p+q+\nu+1 \end{matrix} \right) \right]^2. \quad (37)$$

Proof: By plugging (29) into (64), and using (72), we obtain (37) immediately. □

With Lemmas 4 and 5, the NACF and the correlation coefficient can be calculated according to

$$\tilde{r}_{\mathcal{I}}(i) = \frac{r_{\mathcal{I}}(i)}{\mathbb{E}[\mathcal{I}_l^2]}, \quad (38)$$

and

$$\rho_{\mathcal{I}}(i) = \frac{r_{\mathcal{I}}(i) - \{\mathbb{E}[\mathcal{I}_l]\}^2}{\mathbb{E}[\mathcal{I}_l^2] - \{\mathbb{E}[\mathcal{I}_l]\}^2}, \quad (39)$$

by inserting (36) and (35) into (38), and (36), (35) and (37) into (39), respectively.

In general, it seems difficult to further simplify (36), (35) and (37). However, we note that

$$\ln(1 + \omega x) \approx \begin{cases} \omega x, & \omega \rightarrow 0, \\ \ln(\omega x), & \omega \rightarrow \infty. \end{cases} \quad (40)$$

Using (40), we obtain asymptotic closed-form expressions for the NACF, $\tilde{r}_{\mathcal{I}}(i)$, and the correlation coefficient, $\rho_{\mathcal{I}}(i)$, at low- and high-SNR regimes, as follows.

1) *The Low-SNR Regime:* If $\eta \rightarrow 0$, based on (40), (34) can be approximated by

$$\mathcal{I}_l \approx \sum_{m=1}^M \frac{\eta}{N_T} \lambda_m(l), \quad (41)$$

which is the same as the low-SNR approximation of \mathcal{I}_l in a MIMO system with orthogonal space-time block code (OSTBC) transmission [20], due to $\sum_{m=1}^M \lambda_m(l) = \text{tr}[\mathbf{H}_l \mathbf{H}_l^\dagger] = \|\mathbf{H}_l\|_F^2$. Therefore, the NACF and correlation coefficient of interest are equal to those derived for the OSTBC-MIMO system at low SNRs, as stated in the following proposition.

Proposition 1: At the low-SNR regime, the NACF and the correlation coefficient are given by [20]

$$\tilde{r}_{\mathcal{I}}(i) \approx \frac{N_R N_T + \varrho_i^2}{N_R N_T + 1}, \quad (42)$$

$$\rho_{\mathcal{I}}(i) \approx \varrho_i^2. \quad (43)$$

2) *The High-SNR Regime:* If $\eta \rightarrow \infty$, based on (40), (34) can be approximated by

$$\mathcal{I}_l \approx \sum_{m=1}^M \ln \left[\frac{\eta}{N_T} \lambda_m(l) \right], \quad (44)$$

whose NACF and correlation coefficient are presented in the following theorem.

Theorem 3: At high SNRs, the NACF and the correlation coefficient are given by (45) and (46), respectively

$$\tilde{r}_{\mathcal{I}}(i) \approx \frac{\sum_{m=0}^{M-1} \frac{M!(m+\nu)! \varrho_i^{2(M-m)}}{(M-m)^2 N! m!} {}_4F_3(M-m, M-m, M+1, 1; M-m+1, M-m+1, N+1; \varrho_i^2) + \left(\sum_{m=0}^{M-1} \psi_{N-m} + M \ln \frac{\eta}{N_T} \right)^2}{\sum_{m=0}^{M-1} \zeta(2, N-m) + \left(\sum_{m=0}^{M-1} \psi_{N-m} + M \ln \frac{\eta}{N_T} \right)^2}, \quad (45)$$

$$\rho_{\mathcal{I}}(i) \approx \frac{\sum_{m=0}^{M-1} \frac{M!(m+\nu)! \varrho_i^{2(M-m)}}{(M-m)^2 N! m!} {}_4F_3(M-m, M-m, M+1, 1; M-m+1, M-m+1, N+1; \varrho_i^2)}{\sum_{m=0}^{M-1} \zeta(2, N-m)}, \quad (46)$$

where ${}_pF_q(a_1, \dots, a_p; b_1, \dots, b_q; z)$ is the generalized hypergeometric function [24, pp. 1071, 9.14.1], $\zeta(\cdot, \cdot)$ is the Riemann zeta function, given by $\zeta(z, q) = \sum_{k=0}^{\infty} \frac{1}{(q+k)^z}$ [24, pp. 1101, 9.521.1], and ψ_k is the digamma function [24, pp. 954, 8.365.4].

Proof: See Appendix V. □

Theorem 3 includes the high-SNR approximation for the OSTBC-MIMO system in [20] as a special case. In fact, with $M = 1$, (45) and (46) simplify to the corresponding results in [20] by replacing N with MN , i.e.,

$$\tilde{\rho}_{\mathcal{I}}(i) \approx \frac{\frac{\varrho_i^2}{MN} {}_3F_2(1, 1, 1; 2, MN + 1; \varrho_i^2) + \left(\psi_{MN} + \ln \frac{\eta}{N_T}\right)^2}{\zeta(2, MN) + \left(\psi_{MN} + \ln \frac{\eta}{N_T}\right)^2}, \quad (47)$$

$$\rho_{\mathcal{I}}(i) \approx \frac{\frac{\varrho_i^2}{MN} {}_3F_2(1, 1, 1; 2, MN + 1; \varrho_i^2)}{\zeta(2, MN)}, \quad (48)$$

where the identity ${}_4F_3(1, 1, 1, 2; 2, 2, MN + 1; x) = {}_3F_2(1, 1, 1; 2, MN + 1; x)$ is used.

Based on Theorem 3, we conclude that if $\nu = 0$ and $M \rightarrow \infty$, (46) reduces to

$$\lim_{M \rightarrow \infty} \rho_{\mathcal{I}}(i) = \frac{-\ln(1 - \varrho_i^2)}{\lim_{p \rightarrow \infty} \sum_{k=1}^p \frac{1}{k}} = \delta_{i,0}, \quad (49)$$

where we the first “=” is obtained by collecting the terms in (46), and the second “=” is due to $\varrho_i < 1, i \neq 0$. We conjecture that the second “=” of (49) holds for any finite ν at high SNRs, i.e., $\lim_{M \rightarrow \infty} \rho_{\mathcal{I}}(i) = \delta_{i,0}, \forall \nu < \infty$. It implies that MIMO IMI is asymptotically uncorrelated at high SNRs, if the difference between the numbers of Tx and Rx antennas is finite.

To better understand Theorem 3, the Taylor expansion of (46) and the maximum difference between (43) and (46) is listed in Table I, for different values of M and N . From Table I, the following observations can be made.

- If $\nu = N - M$ is fixed, the maximum difference between the low- and high-SNR approximations increases when M increases, which is supported by the first four rows of Table I, i.e., $(M, N) = (1, 1), (2, 2), (3, 3)$, and $(4, 4)$.
- From the last several rows of Table I, i.e., $(M, N) = (4, 4), (4, 8), (4, 12)$ and $(4, 16)$, one may conclude that if M is fixed, the maximum difference between the low- and high-SNR approximations decreases as ν increases. Furthermore, $\rho_{\mathcal{I}}(i)$ can be well approximated by ϱ_i^2 , with negligible error for any SNR, when $\frac{\nu}{M}$ is not small.

B. LCR and AOD of MIMO IMI

The technique developed in Subsection III-B is also valid for calculating the LCR and AOD of MIMO IMI, i.e., we can obtain them by replacing $\phi_{\lambda}(\lambda_{\text{th}})$ and $\varphi_{\lambda}(\lambda_{\text{th}})$ with $\phi_{\mathcal{I}}(I_{\text{th}}) = P_r\{\mathcal{I}_l > I_{\text{th}}\}$ and $\varphi_{\mathcal{I}}(I_{\text{th}}) = P_r\{\mathcal{I}_l > I_{\text{th}}, \mathcal{I}_{l-1} > I_{\text{th}}\}$ in (25) and (31), respectively. Therefore, we only need to calculate, $\phi_{\mathcal{I}}(I_{\text{th}})$ and $\varphi_{\mathcal{I}}(I_{\text{th}})$, which are presented in the following theorem.

Theorem 4: At any given level I_{th} , $\phi_{\mathcal{I}}(I_{\text{th}})$ and $\varphi_{\mathcal{I}}(I_{\text{th}})$ can be expressed in terms of multiple integrals, given

by (50) and (51), respectively.

$$\begin{aligned} \phi_{\mathcal{I}}(I_{\text{th}}) &= \underbrace{\int \cdots \int_{\prod_{m=1}^M \left(1 + \frac{\eta x_m}{N_T}\right) > \exp(I_{\text{th}})}}_{M! \prod_{m=0}^{M-1} m!(m+\nu)! \exp\left(\sum_{m=1}^M x_m\right)} \frac{\prod_{m=1}^M x_m^\nu \prod_{m < n}^M (x_m - x_n)^2}{\prod_{m=1}^M dx_m}, \quad (50) \\ \varphi_{\mathcal{I}}(I_{\text{th}}) &= \underbrace{\int \cdots \int_{\prod_{m=1}^M \left(1 + \frac{\eta x_m}{N_T}\right) > \exp(I_{\text{th}})} \int \cdots \int_{\prod_{m=1}^M \left(1 + \frac{\eta y_m}{N_T}\right) > \exp(I_{\text{th}})}}_{M! M! \prod_{m=0}^{M-1} m!(m+\nu)! \varrho_1^{MN-M} (1 - \varrho_1^2)^M \exp\left(\sum_{m=1}^M \frac{x_m + y_m}{1 - \varrho_1^2}\right)} \frac{\prod_{m < n}^M [(x_m - x_n)(y_m - y_n)]^2 \prod_{m=1}^M (\sqrt{x_m y_m})^\nu \det \left| I_\nu \left(\frac{2\varrho_1 \sqrt{x_m y_n}}{1 - \varrho_1^2} \right) \right|}{\prod_{m=1}^M dx_m dy_m}. \quad (51) \end{aligned}$$

Proof: Let $\{X_m\}_{m=1}^M$ and $\{Y_m\}_{m=1}^M$ be M unordered eigenvalues of $\mathbf{H}(l)\mathbf{H}^\dagger(l)$ and $\mathbf{H}(l-1)\mathbf{H}^\dagger(l-1)$, respectively. Then the joint PDF of $\{X_m\}_{m=1}^M$ is given by $p(x_1, x_2, \dots, x_M)$ in (50) [30], and the joint PDF of $\{X_m\}_{m=1}^M$ and $\{Y_m\}_{m=1}^M$ is given by $p(x_1, x_2, \dots, x_M, y_1, y_2, \dots, y_M)$ in (51) [23]. Moreover, according to (34), the event $\{\mathcal{I}_l > I_{\text{th}}\}$ is equivalent to $\left\{ \prod_{m=1}^M \left(1 + \frac{\eta X_m}{N_T}\right) > e^{I_{\text{th}}} \right\}$, which leads to (50). Similarly, it is straightforward to see that the two events $\{\mathcal{I}_l > I_{\text{th}}, \mathcal{I}_{l-1} > I_{\text{th}}\}$ and $\left\{ \prod_{m=1}^M \left(1 + \frac{\eta X_m}{N_T}\right) > e^{I_{\text{th}}}, \prod_{m=1}^M \left(1 + \frac{\eta Y_m}{N_T}\right) > e^{I_{\text{th}}} \right\}$, have the same probability, which results in (51). \square

Although (50) and (51) can be used to calculate the LCR and AOD of MIMO IMI for small M 's, e.g., $M = 2$, via numerical multiple integrals, it is impractical for large M 's. Fortunately, we can approximate \mathcal{I}_l as a Gaussian random variable for large M 's and N 's, which is summarized in the following proposition.

Proposition 2: If M and N are large, \mathcal{I}_l can be approximated as a Gaussian random variable with mean $\mu_{\mathcal{I}} = \mathbb{E}[\mathcal{I}_l]$ and variance $\sigma_{\mathcal{I}}^2 = \mathbb{E}[\mathcal{I}_l^2] - \{\mathbb{E}[\mathcal{I}_l]\}^2$, where $\mathbb{E}[\mathcal{I}_l]$ and $\mathbb{E}[\mathcal{I}_l^2]$ are given by (35) and (36), respectively [16]–[18]. Moreover, we approximate \mathcal{I}_l and \mathcal{I}_{l-i} by a bivariate Gaussian random vector with mean $(\mathbb{E}[\mathcal{I}_l], \mathbb{E}[\mathcal{I}_l])^T$ and the covariance matrix $\Sigma_{\mathcal{I}} = \sigma_{\mathcal{I}}^2 \begin{pmatrix} 1 & \rho_{\mathcal{I}}(i) \\ \rho_{\mathcal{I}}(i) & 1 \end{pmatrix}$, where $\rho_{\mathcal{I}}(i)$ is presented in (39).

Based on Proposition 2, we have the following theorem for the LCR and AOD of MIMO IMI.

Theorem 5: Using the Gaussian approximation, we can express the LCR and AOD of MIMO IMI as

$$N_{\mathcal{I}}(I_{\text{th}}) = \frac{1}{\pi T_s} \int_{\frac{\pi}{4} + \arcsin[\rho_{\mathcal{I}}(1)]}^{\frac{\pi}{2}} \exp\left(-\frac{\tilde{I}_{\text{th}}^2}{2 \sin^2 \theta}\right) d\theta, \quad (52)$$

$$\bar{t}_{\mathcal{I}}(I_{\text{th}}) = \frac{1 - Q\left(\tilde{I}_{\text{th}}\right)}{N_{\mathcal{I}}(I_{\text{th}})}, \quad (53)$$

where $\tilde{I}_{\text{th}} = \frac{I_{\text{th}} - \mu_{\mathcal{I}}}{\sigma_{\mathcal{I}}}$ is the normalized threshold, and $Q(x) = \frac{1}{\sqrt{2\pi}} \int_x^\infty e^{-\frac{t^2}{2}} dt$ is the Gaussian Q -function.

Proof: See Appendix VI. \square

Theorem 5 requires $\mu_{\mathcal{I}}$, $\sigma_{\mathcal{I}}^2$ and $\rho_{\mathcal{I}}(1)$, which can be obtained from (35), (36) and (39). However, for low and high SNRs, we may use their corresponding approximations. For high SNRs, they are given by (79), (80) and (46), whereas for low SNRs we have $\mu_{\mathcal{I}} = \eta N_R$, $\sigma_{\mathcal{I}}^2 = \frac{\eta^2 N_R}{N_T}$ [20], and $\rho_{\mathcal{I}}(1) = \varrho_1^2$, obtained from (43). In practice, the LCR and AOD at $\mu_{\mathcal{I}}$, the ergodic capacity, are of interest, which simplify Theorem 5 considerably.

Corollary 1: The LCR and AOD of MIMO IMI at the level $\mu_{\mathcal{I}}$ are, respectively, given by

$$N_{\mathcal{I}}(\mu_{\mathcal{I}}) = \frac{\pi - 2 \arcsin[\rho_{\mathcal{I}}(1)]}{4\pi T_s}, \quad (54)$$

$$\bar{t}_{\mathcal{I}}(\mu_{\mathcal{I}}) = \frac{2\pi T_s}{\pi - 2 \arcsin[\rho_{\mathcal{I}}(1)]}. \quad (55)$$

V. NUMERICAL RESULTS AND DISCUSSION

In this paper, a generic power spectrum [19, (8)] [20] is used to simulate time-varying Rayleigh flat fading channels with *nonisotropic* scattering, according to the spectral method [31]. Similar to [20], to verify the accuracy of the derived formulas, we consider two types of scattering environments: *isotropic* scattering and *nonisotropic* scattering with three clusters of scatterers. For *nonisotropic* scattering, parameters of the three clusters are given by $[P_1, \kappa_1, \theta_1] = [\frac{1}{3}, 6, 0]$, $[P_2, \kappa_2, \theta_2] = [\frac{1}{2}, 6, \frac{\pi}{4}]$, and $[P_3, \kappa_3, \theta_3] = [\frac{1}{6}, 8, \frac{25\pi}{18}]$, respectively. In addition, in all the simulations, the maximum Doppler frequency f_D is set to 10Hz, and $T_s = \frac{1}{20f_D}$ seconds. The AoA distributions and the corresponding channel correlation coefficients for the above two scattering environments are plotted in Fig. 2.

In the following subsections, Monte Carlo simulations are performed to verify NACF, the correlation coefficient, LCR and AFD of *eigen*-channels and the MIMO IMI of two MIMO systems in the above two propagation environments: one is 4×4 and the other is 12×3 . The NACF and the correlation coefficient bear almost the same information. The same comment applies to LCR and AFD. Therefore, we only report the simulation results for the correlation coefficient and the LCR, to save space.

A. Eigen-Channels

In this subsection, the correlation coefficient and the LCR of *eigen*-channels are considered for both isotropic and nonisotropic scattering environments.

1) *Isotropic Scattering:* This is Clarke's model [10], with uniform AoA. The comparison between the simulation and theoretical results is given in Fig. 3.

2) *Nonisotropic Scattering:* This is a general case, with an arbitrary AoA distribution [19][20]. The comparison results are presented in Fig. 4.

In Figs. 3 and 4, the upper left and right subfigures show the correlation coefficient and the LCR of *eigen*-channels in a 4×4 MIMO system, respectively, whereas the lower left and right subfigures show the results in a 12×3 MIMO system. In all figures, "Simu." means simulation. In the correlation coefficient plots, "Theo." means they are calculated according to (18), and " $(k = l)$ " denotes the autocorrelation coefficient, whereas " $(k \neq l)$ " indicates the cross-correlation coefficient. In the LCR plots, "Theo" indicates that the curve is computed using (25)-(28).

Based on the plots in Figs. 3 and 4, we can see that the derived analytical formulas perfectly match Monte Carlo simulations.

B. MIMO IMI

In this subsection, the correlation coefficient and the LCR of MIMO IMI are presented for both isotropic and nonisotropic scattering environments at low- and high-SNR regimes. In the simulations and theoretical calculations, we set $\eta = -20$ dB for low SNR, and $\eta = 30$ dB for high SNR.

1) *Isotropic Scattering*: For this case, the comparison results are shown in Fig. 5.

2) *Nonisotropic Scattering*: The comparison results regarding nonisotropic scattering are given in Fig. 6.

In Figs. 5 and 6, the upper three subfigures present the correlation coefficient and the LCR of the MIMO IMI in a 4×4 system. Specifically, the upper left subfigure shows the correlation coefficient at low- and high-SNR regimes, the upper middle subfigure gives the LCR of the MIMO IMI at the low-SNR regime, whereas the upper right gives the LCR at the high-SNR regime. In addition, the lower three subfigures present the corresponding results in the 12×3 system. In the correlation coefficient plots, ‘‘Theo. (Low SNR)’’ corresponds to (43), whereas ‘‘Theo. (High SNR)’’ corresponds to (46). In the LCR plots, ‘‘Theo.’’ means the values are computed from (52), where we used low- and high-SNR approximations for the mean $\mu_{\mathcal{I}}$ and variance $\sigma_{\mathcal{I}}^2$, listed immediately after Theorem 5.

From Figs. 5 and 6, the following observations can be made.

- **Correlation coefficient**: If $\nu = \max(N_T, N_R) - \min(N_T, N_R)$ is large compared to $M = \min(N_T, N_R)$, we can approximate the correlation coefficient of MIMO IMI by the squared amplitude of the channel correlation coefficient for all SNRs, since low- and high-SNR approximations are very close to each other (see the results for the 12×3 system). However, if ν is small compared to M , the gap between the low- and high-SNR approximations is large (see the results for the 4×4 system). Therefore, we need to resort to the exact formulas in (36), (35), (37) and (39) to calculate the accurate values of the correlation coefficient, for not so small or large SNRs. For example, at $\eta = 15$ dB, the simulation and exact theoretical curves, as well as low- and high-SNR approximations are shown in Fig. 7, for the correlation coefficient of the MIMO IMI in a 4×4 system.
- **LCR**: The Gaussian approximation works well at both low and high SNRs in large MIMO systems, e.g., the considered 12×3 channel. But it is not the case in small MIMO systems, say 4×4 , where the Gaussian approximation has an obvious deviation from the simulation result at high SNR. This is because the central limit theorem does not hold for IMI in small MIMO systems⁵. For this case, we can numerically compute the multiple integrals given in (50) and (51), to calculate the LCR.
- **LCR**: Compared Fig. 3 and Fig. 4, we find the LCR of an eigen-channel is not sensitive to the scattering environment, which is not the case for the LCR of MIMO IMI. Furthermore, based on Figs. 5 and 6, we can see that the IMI in a nonisotropic scattering environment has less fluctuations than that in the isotropic scattering scenario.

⁵In fact, there are obvious differences between the true PDF and the Gaussian approximation in Fig. 1 of [17] at $\eta = 15$ dB. Larger deviations are also observed at higher SNRs, say, $\eta = 20$ dB, in Fig. 1 of [17].

VI. CONCLUSION

In this paper, closed-form expressions for several key second-order statistics such as the autocorrelation function, the correlation coefficient, level crossing rate and average fade/outage duration of *eigen*-channels and the instantaneous mutual information (IMI) are derived in MIMO time-varying Rayleigh flat fading channels.

Simulation and analytical results show that the eigen-modes tend to be spatio-temporally uncorrelated in large MIMO systems, and the correlation coefficient of the IMI can be well approximated by the squared amplitude of the correlation coefficient of the channel, if the difference between the number of Tx and Rx antennas is much larger than the minimum number of Tx and Rx antennas. In addition, we have also observed that the LCR of an eigen-mode is less sensitive to the scattering environment than the IMI.

The analytical expressions, supported by Monte Carlo simulations, provide quantitative information regarding the dynamic behavior of MIMO channels. They also serve as useful tools for MIMO system designs. For example, one may improve the performance of the feedbacked-IMI-based rate scheduler in a multiuser MIMO system by exploiting the temporal correlation of the IMI of each user.

APPENDIX I

PROOF OF LEMMA 1

Although the mean and second moment of $\lambda_m(l)$ were respectively given by (57) and (58) in [16] via a smart indirect method, we calculate them directly using its marginal PDF in (7), as follows.

Using 8.902.2 [24, pp. 1043], we can rewrite (7) as

$$p(x) = \frac{(M-1)!x^\nu}{(M+\nu-1)!e^x} \left\{ [L_{M-1}^\nu(x)]' L_M^\nu(x) - [L_M^\nu(x)]' L_{M-1}^\nu(x) \right\}, \quad (56)$$

where ' mean the derivative with respect to x . With [24, pp. 1062, 8.971.2]

$$[L_n^\nu(x)]' = -L_{n-1}^{\nu+1}(x) \quad (57)$$

and [24, pp. 1062, 8.971.5]

$$L_n^k(x) = L_n^{k+1}(x) - L_{n-1}^{k+1}(x), \quad (58)$$

(56) further reduces to

$$p(x) = \frac{(M-1)!x^\nu}{(M+\nu-1)!e^x} \left\{ [L_{M-1}^{\nu+1}(x)]^2 - L_M^{\nu+1}(x)L_{M-2}^{\nu+1}(x) \right\}, \quad (59)$$

where the convention $L_m^k(x) = 0, m < 0$ should be used when it is applicable.

Using (59), we obtain $\mathbb{E}[\lambda_m(l)]$ as

$$\begin{aligned} \mathbb{E}[\lambda_m(l)] &= \int_0^\infty xp(x)dx, \\ &= \frac{(M-1)!}{(M+\nu-1)!} \left\{ \int_0^\infty x^{\nu+1} e^{-x} [L_{M-1}^{\nu+1}(x)]^2 dx - \int_0^\infty x^{\nu+1} e^{-x} L_M^{\nu+1}(x)L_{M-2}^{\nu+1}(x) dx \right\}, \\ &= M + \nu, \end{aligned} \quad (60)$$

where the orthogonality of Laguerre polynomials [32, pp. 267, 7.414.3] is used, i.e.

$$\int_0^\infty e^{-x} x^\nu L_k^\nu(x) L_l^\nu(x) dx = \frac{(k+\nu)!}{k!} \delta_{k,l}. \quad (61)$$

The last line results in (13), considering $N = M + \nu$.

By substituting (58) with $k = \nu + 1$ into (59) and using (61), we can easily obtain (14).

APPENDIX II PROOF OF LEMMA 2

A. *The case of $i = 0$*

For $i = 0$, the value of $\mathbb{E}[\lambda_m^2(l)]$ is given in (14).

B. *The case of $i \neq 0$*

For $i \neq 0$, we need the following two lemmas.

Lemma 6: While j, k and ν are non-negative integers, the value of the integral,

$I_1(j, k, \nu) = \int_0^\infty x^{\nu+1} e^{-x} L_j^\nu(x) L_k^\nu(x) dx$, is given by

$$I_1(j, k, \nu) = \begin{cases} \frac{(2k+\nu+1)(k+\nu)!}{k!}, & |j - k| = 0, \\ -\frac{[\min(j,k)+\nu+1]!}{[\min(j,k)]!}, & |j - k| = 1, \\ 0, & |j - k| \geq 2. \end{cases} \quad (62)$$

Proof: Using (58), we have

$$L_j^\nu(x) L_k^\nu(x) = L_j^{\nu+1}(x) L_k^{\nu+1}(x) + L_{j-1}^{\nu+1}(x) L_{k-1}^{\nu+1}(x) - L_j^{\nu+1}(x) L_{k-1}^{\nu+1}(x) - L_{j-1}^{\nu+1}(x) L_k^{\nu+1}(x). \quad (63)$$

Substitution of (63) into $I_1(j, k, \nu)$ results in (62), with the aid of (61) and the convention $L_m^k(x) = 0, m < 0$. \square

Lemma 7: The joint PDF in (6) can be written in the following equivalent form

$$p(x, y) = \frac{1}{M^2} \sum_{j=M}^{\infty} \sum_{k=0}^{M-1} \left[\frac{j!k!}{(j+\nu)!(k+\nu)!} \rho_i^{2(j-k)} \frac{x^\nu y^\nu}{e^{x+y}} L_j^\nu(x) L_j^\nu(y) L_k^\nu(x) L_k^\nu(y) \right] + p(x)p(y), \quad (64)$$

where $p(\cdot)$ is the marginal PDF given by (7).

Proof: By applying the Hille-Hardy formula [32, pp. 185, (46)]

$$\sum_{k=0}^{\infty} \frac{k!z^k}{(k+\nu)!} L_k^\nu(x) L_k^\nu(y) = \frac{(xyz)^{-\frac{k}{2}}}{1-z} \exp\left(-z \frac{x+y}{1-z}\right) I_\nu\left(\frac{2\sqrt{xyz}}{1-z}\right), |z| < 1, \quad (65)$$

to (6), we can obtain (64) after some algebraic manipulations. \square

Using Lemmas 6 and 7, it is straightforward to obtain

$$r_{m,m}(i) = \frac{1}{M^2} \frac{M!(M-1)! \rho_i^2}{(M+\nu)!(M+\nu-1)!} [I_1(M, M-1, \nu)]^2 + N^2, \quad (66)$$

which reduces to (15), based on (62) and $N = M + \nu$.

APPENDIX III
PROOF OF LEMMA 3

A. The case of $i = 0$

For $i = 0$, we need the following proposition.

Proposition 3: If (x_1, x_2) are a pair of eigenvalues, randomly selected from $\{\lambda_m(l)\}_{m=1}^M$, then their joint PDF is given by [23]

$$p(x_1, x_2) = \frac{(x_1 x_2)^\nu e^{-(x_1 + x_2)}}{M(M-1)} \sum_{\substack{p, q=0 \\ p \neq q}}^{M-1} \frac{p!q!}{(p+\nu)!(q+\nu)!} \left\{ [L_p^\nu(x_1)L_q^\nu(x_2)]^2 - L_p^\nu(x_1)L_q^\nu(x_1)L_p^\nu(x_2)L_q^\nu(x_2) \right\}. \quad (67)$$

Note that (67) is different from (6). By reordering the items, we can rewrite (67) as

$$p(x_1, x_2) = \frac{M}{M-1} p(x_1)p(x_2) - \frac{(x_1 x_2)^\nu e^{-(x_1 + x_2)}}{M(M-1)} \sum_{j=0}^{M-1} \sum_{k=0}^{M-1} \frac{j!k!}{(j+\nu)!(k+\nu)!} L_j^\nu(x_1)L_k^\nu(x_1)L_j^\nu(x_2)L_k^\nu(x_2). \quad (68)$$

Using Lemma 6 and (68), it is easy to obtain

$$r_{m,n}(i) = \frac{M}{M-1} N^2 - \frac{S}{M(M-1)}, \quad (69)$$

where $S = \sum_{j=0}^{M-1} \sum_{k=0}^{M-1} \frac{j!k![L_1(j,k,\nu)]^2}{(j+\nu)!(k+\nu)!}$. According to (62), we have

$$\begin{aligned} S &= \sum_{k=0}^{M-1} (2k+\nu+1)^2 + 2 \sum_{k=0}^{M-2} (k+1)(k+\nu+1), \\ &= MN(M+N-1), \end{aligned} \quad (70)$$

where the last line is derived based on $\sum_{k=0}^n k = \frac{n(n+1)}{2}$ [24, pp. 2, 0.121.1] and $\sum_{k=0}^n k^2 = \frac{n(n+1)(2n+1)}{6}$ [24, pp. 2, 0.121.2].

Substitution of (70) into (69) proves the first part of Lemma 3, i.e., $i = 0$. Note that the same result was derived in Lemma A of [16] via an indirect method.

B. The case of $i \neq 0$

Note that $\{\lambda_m(l)\}_{m=1}^M$ and $\{\lambda_m(l-i)\}_{m=1}^M$ are unordered eigenvalues of $\mathbf{H}(l)\mathbf{H}^\dagger(l)$ and $\mathbf{H}(l-i)\mathbf{H}^\dagger(l-i)$, respectively, for $i \neq 0$. So the bivariate PDF of $\{\lambda_m(l), \lambda_n(l-i)\}$, $m \neq n$, is the same as that of $\{\lambda_m(l), \lambda_m(l-i)\}$, the latter given in (6). Therefore, $r_{m,n}(i) = r_{m,m}(i)$, $i \neq 0, \forall m, n$, where $r_{m,m}(i) = N^2 + \frac{Nq_i^2}{M}$, $i \neq 0$, is proved in Appendix II.

APPENDIX IV
PROOF OF LEMMA 4

According to (34), we have

$$\begin{aligned} \mathbb{E}[\mathcal{I}_l] &= M \mathbb{E} \left[\ln \left(1 + \frac{\eta}{N_T} \lambda_m(l) \right) \right], \\ &= M \int_0^\infty \ln \left(1 + \frac{\eta}{N_T} x \right) p(x) dx, \end{aligned} \quad (71)$$

where $p(x)$ is given in (7). Substitution of (7) and (29) into (71) results in (35), with the aid of the following integral identity [20, (67)]

$$\int_0^\infty x^k e^{-x} \ln(1+\omega x) dx = G_{2,3}^{3,1} \left(\frac{1}{\omega} \left| \begin{matrix} 0, 1 \\ 0, 0, k+1 \end{matrix} \right. \right), \quad (72)$$

where G is Meijer's G function [24, pp. 1096, 9.301].

Similarly, we have

$$\begin{aligned} \mathbb{E}[\mathcal{I}_l^2] &= M \mathbb{E} \left[\ln^2 \left(1 + \frac{\eta}{N_T} \lambda_m(l) \right) \right] + \underbrace{M(M-1) \mathbb{E} \left[\ln \left(1 + \frac{\eta}{N_T} \lambda_m(l) \right) \ln \left(1 + \frac{\eta}{N_T} \lambda_n(l) \right) \right]}_{m \neq n}, \\ &= M \int_0^\infty \ln^2 \left(1 + \frac{\eta}{N_T} x \right) p(x) dx + M(M-1) \int_0^\infty \int_0^\infty \ln \left(1 + \frac{\eta}{N_T} x_1 \right) \ln \left(1 + \frac{\eta}{N_T} x_2 \right) p(x_1, x_2) dx_1 dx_2, \end{aligned} \quad (73)$$

where $p(x)$ and $p(x_1, x_2)$ are given in (7) and (68), respectively. Substitution of (7), (29) and (68) into (73) leads us to (36), upon using (72) and the following integral equality [20, (69)]

$$\int_0^\infty x^k e^{-x} \ln^2(1+\omega x) dx = 2e^{\frac{1}{\omega}} \omega^{-(k+1)} \sum_{j=0}^k \binom{k}{j} (-1)^{k-j} G_{3,4}^{4,0} \left(\frac{1}{\omega} \left| \begin{matrix} -j, -j, -j \\ 0, -j-1, -j-1, -j-1 \end{matrix} \right. \right). \quad (74)$$

APPENDIX V

PROOF OF THEOREM 3

First we derive the expressions for the first and second moments of \mathcal{I}_l in (44), based on the following lemma.

Lemma 8: Let $\mathbf{X} = (x_{m,n})$ be a random matrix with M rows and N columns, $M \leq N$, where each element is a zero mean unit variance complex Gaussian random variable and all the N columns are i.i.d M -variate random vectors with the same $M \times M$ positive definite covariance matrix Σ . The mean and variance of $\ln \det(\mathbf{X}\mathbf{X}^\dagger)$ are

$$\mathbb{E} [\ln \det(\mathbf{X}\mathbf{X}^\dagger)] = \sum_{m=0}^{M-1} \psi_{N-m} + \ln \det \Sigma, \quad (75)$$

$$\text{var} [\ln \det(\mathbf{X}\mathbf{X}^\dagger)] = \sum_{m=0}^{M-1} \zeta(2, N-m). \quad (76)$$

Proof: According to Theorem 1.1 of [33], $\frac{\det(\mathbf{X}\mathbf{X}^\dagger)}{2^{-M} \det \Sigma}$ has the same distribution as the product of M independent χ^2 random variables with $2N, 2(N-1), \dots, 2(N-M+1)$ degrees of freedom, respectively. Therefore, we can express $\ln \det(\mathbf{X}\mathbf{X}^\dagger)$ as

$$\ln \det(\mathbf{X}\mathbf{X}^\dagger) \stackrel{d}{=} \sum_{m=0}^{M-1} \ln \left(\sqrt[M]{\det \Sigma} y_m \right), \quad (77)$$

where the notation $\stackrel{d}{=}$ indicates “equal to in distribution”, $2y_m$ is a χ^2 random variable with $2(N-m)$ degrees of freedom, and $\{y_m\}_{m=0}^{M-1}$ are independent.

Based on the results in [20], we have $\mathbb{E} [\ln y_m] = H_{N-m-1} - \mathbf{C}$ and $\text{var} [\ln y_m] = \zeta(2, N-m)$, where H_k is the k^{th} harmonic number [34, pp. 29, (2.13)], defined by $H_k = \sum_{j=1}^k \frac{1}{j}$ for $k \geq 1$ with $H_0 = 0$, and $\mathbf{C} = 0.577215 \dots$

is the Euler-Mascheroni constant [24, pp. xxx]. This completes the proof if we note $\psi_{k+1} = H_k - \mathbf{C}$ [24, pp. 952, 8.365.4].

It is interesting to observe that the correlation matrix Σ affects the mean of $\ln \det (\mathbf{X}\mathbf{X}^\dagger)$ in (75), but has no impact on its variance in (76). \square

According to Theorem 1.1.2 of [35] we have

$$\prod_{m=1}^M \lambda_m(l) = \begin{cases} \det (\mathbf{H}_l \mathbf{H}_l^\dagger), & N_R \leq N_T, \\ \det (\mathbf{H}_l^\dagger \mathbf{H}_l), & N_R > N_T. \end{cases} \quad (78)$$

By applying Lemma 8 and (78) to (44) with $\Sigma = \mathbf{I}_M$, it is straightforward to write the mean and variance of \mathcal{I}_l as

$$\mathbb{E}[\mathcal{I}_l] \approx \sum_{m=0}^{M-1} \psi_{N-m} + M \ln \frac{\eta}{N_T}, \quad (79)$$

and

$$\text{var}[\mathcal{I}_l] \approx \sum_{m=0}^{M-1} \zeta(2, N-m), \quad (80)$$

respectively. These two are consistent with the results in [16], where an implicit complex extension of Theorem 3.3.4 of [35] was used. Clearly, the second moment of \mathcal{I}_l is given by

$$\mathbb{E}[\mathcal{I}_l^2] \approx \sum_{m=0}^{M-1} \zeta(2, N-m) + \left(\sum_{m=0}^{M-1} \psi_{N-m} + M \ln \frac{\eta}{N_T} \right)^2. \quad (81)$$

For calculating the autocorrelation of \mathcal{I}_l , we need the following lemma.

Lemma 9: With j, k and ν as non-negative integers and $j \neq k$, the value of the integral $I_2(j, k, \nu) = \int_0^\infty (\ln x) x^\nu e^{-x} L_j^\nu(x) L_k^\nu(x) dx$ is given by

$$I_2(j, k, \nu) = \frac{[\min(j, k) + \nu]!}{[\min(j, k)]! [\min(j, k) - \max(j, k)]}. \quad (82)$$

Proof: First we consider $j > k$. Substitution of $L_k^\nu(x)$ with (29) into $I_2(j, k, \nu)$ gives

$$\begin{aligned} I_2(j, k, \nu) &= \sum_{p=0}^k \binom{k+\nu}{k-p} \frac{(-1)^p}{p!} \int_0^\infty (\ln x) x^{p+\nu} e^{-x} L_j^\nu(x) dx, \\ &= \sum_{p=0}^k \binom{k+\nu}{k-p} \frac{(-1)^p}{p!} \frac{(-1)^{p-1} p! (j-p-1)! (p+\nu)!}{j!}, \\ &= -\frac{(k+\nu)!}{j!} \sum_{p=0}^k \frac{(j-p-1)!}{(k-p)!}, \end{aligned} \quad (83)$$

where the second line comes from 2.19.6.2 [36, pp. 469]. Using $\sum_{q=0}^m \binom{n+q}{n} = \binom{n+m+1}{n+1}$ [24, pp. 4, 0.151.1], we have $\sum_{p=0}^k \frac{(j-p-1)!}{(k-p)!} \stackrel{q=k-p}{=} \sum_{q=0}^k \frac{(j-k-1-q)!}{j-k-1} (j-k-1)! = \binom{j}{j-k} (j-k-1)! = \frac{j!}{k!(j-k)}$, which reduces (83) to

$$I_2(j, k, \nu) = \frac{(k+\nu)!}{k!(k-j)}. \quad (84)$$

Similarly, for $j < k$, we obtain

$$I_2(j, k, \nu) = \frac{(j+\nu)!}{j!(j-k)}. \quad (85)$$

Combination of (84) and (85) results in (82). \square

Now we proceed to prove (45) and (46). Based on the high-SNR approximation of \mathcal{I}_l in (44), we have

$$\begin{aligned} r_{\mathcal{I}}(i) &\approx \sum_{m=1}^M \sum_{n=1}^M \mathbb{E} \left[\ln \frac{\eta \lambda_m(l)}{N_T} \ln \frac{\eta \lambda_n(l-i)}{N_T} \right], \\ &= M^2 \mathbb{E} \left[\ln \frac{\eta \lambda_1(l)}{N_T} \ln \frac{\eta \lambda_1(l-i)}{N_T} \right], \\ &= M^2 \left[\ln^2 \frac{\eta}{N_T} + 2 \ln \frac{\eta}{N_T} \mathbb{E}[\ln \lambda(l)] + r_{\ln \lambda}(i) \right], \end{aligned} \quad (86)$$

where $r_{\ln \lambda}(i) = \mathbb{E}[\ln \lambda(l) \ln \lambda(l-i)]$. Using (64) and Lemma 9, $r_{\ln \lambda}(i)$ can be evaluated as

$$r_{\ln \lambda}(i) = \frac{1}{M^2} \sum_{j=M}^{\infty} \sum_{k=0}^{M-1} \frac{j!k! \varrho_i^{2(j-k)} I_2^2(j, k, \nu)}{(j+\nu)!(k+\nu)!} + \{\mathbb{E}[\ln \lambda(l)]\}^2. \quad (87)$$

By substituting (82) and (87) into (86), we obtain

$$r_{\mathcal{I}}(i) \approx \sum_{k=0}^{M-1} S(k, \nu, \varrho_i) + \{\mathbb{E}[\mathcal{I}_l]\}^2, \quad (88)$$

where $S(k, \nu, \varrho_i) = \sum_{j=M}^{\infty} \frac{j!(k+\nu)! \varrho_i^{2(j-k)}}{k!(j+\nu)!(j-k)!}$, and $\mathbb{E}[\mathcal{I}_l] \approx M \mathbb{E} \left[\ln \frac{\eta \lambda(l)}{N_T} \right]$ is approximated by (79). By introducing a new variable $p = j - M$ in $S(k, \nu, \varrho_i)$ and using the Pochhammer symbol $(x)_n = x(x+1) \cdots (x+n-1)$, we can rewrite $S(k, \nu, \varrho_i)$ as

$$\begin{aligned} S(k, \nu, \varrho_i) &= \frac{M!(k+\nu)! \varrho_i^{2(M-k)}}{(M-k)^2 N! k!} \sum_{p=0}^{\infty} \frac{[(M-k)_p]^2 (M+1)_p (1)_p \varrho_i^{2p}}{[(M-k+1)_p]^2 (N+1)_p p!}, \\ &= \frac{M!(k+\nu)! \varrho_i^{2(M-k)}}{(M-k)^2 N! k!} {}_4F_3(M-k, M-k, M+1, 1; M-k+1, M-k+1, N+1; \varrho_i^2), \end{aligned} \quad (89)$$

where $N = M + \nu$, and the last line comes from the definition of the generalized hypergeometric function [24, pp. 1071, 9.14.1].

Substitution of (81), (88) and (89) into (38) results in (45). Similarly, with (79), (80), (88) and (89), (39) reduces to (46).

APPENDIX VI

PROOF OF THEOREM 5

To simplify the notation, we set $X = \mathcal{I}_l$, $Y = \mathcal{I}_{l-1}$, and $\rho = \rho_{\mathcal{I}}(1)$. According to Proposition 2, we have the PDF of X and the joint PDF of X and Y as

$$p(x) = \frac{1}{\sqrt{2\pi}\sigma_{\mathcal{I}}} \exp \left[-\frac{(x - \mu_{\mathcal{I}})^2}{2\sigma_{\mathcal{I}}^2} \right], \quad (90)$$

and

$$p(x, y) = \frac{\exp \left[-\frac{(x - \mu_{\mathcal{I}})^2 + (y - \mu_{\mathcal{I}})^2 - 2\rho(x - \mu_{\mathcal{I}})(y - \mu_{\mathcal{I}})}{2\sigma_{\mathcal{I}}^2(1 - \rho^2)} \right]}{\sqrt{2\pi(1 - \rho^2)}\sigma_{\mathcal{I}}}. \quad (91)$$

In what follows, we calculate $\phi_{\mathcal{I}}(I_{\text{th}}) = \int_{I_{\text{th}}}^{\infty} p(x) dx$ and $\varphi_{\mathcal{I}}(I_{\text{th}}) = \int_{I_{\text{th}}}^{\infty} \int_{I_{\text{th}}}^{\infty} p(x, y) dx dy$ for the cases of $I_{\text{th}} \geq \mu_{\mathcal{I}}$ and $I_{\text{th}} < \mu_{\mathcal{I}}$.

A. The Case of $I_{\text{th}} \geq \mu_{\mathcal{I}}$

According to (4.2) [26] we obtain

$$\phi_{\mathcal{I}}(I_{\text{th}}) \stackrel{I_{\text{th}} \geq \mu_{\mathcal{I}}}{=} \frac{1}{\pi} \int_0^{\frac{\pi}{2}} \exp\left(-\frac{\tilde{I}_{\text{th}}^2}{2 \sin^2 \theta}\right) d\theta, \quad (92)$$

where $\tilde{I}_{\text{th}} = \frac{I_{\text{th}} - \mu_{\mathcal{I}}}{\sigma_{\mathcal{I}}}$. Similarly, using (4.18) [26] and the following equality

$$\arctan\left(\sqrt{\frac{1+\rho}{1-\rho}}\right) = \frac{\pi}{4} + \frac{\arcsin(\rho)}{2}, \quad (93)$$

we obtain

$$\varphi_{\mathcal{I}}(I_{\text{th}}) \stackrel{I_{\text{th}} \geq \mu_{\mathcal{I}}}{=} \frac{1}{\pi} \int_0^{\frac{\pi}{4} + \frac{\arcsin(\rho)}{2}} \exp\left(-\frac{\tilde{I}_{\text{th}}^2}{2 \sin^2 \theta}\right) d\theta. \quad (94)$$

Substitution of (92) and (94) into (25) results in (52). Moreover, $F_{\mathcal{I}}(I_{\text{th}}) = \int_{-\infty}^{I_{\text{th}}} p(x) dx = 1 - Q(\tilde{I}_{\text{th}})$. By plugging $F_{\mathcal{I}}(I_{\text{th}})$ and (52) into (31) we obtain (53).

B. The Case of $I_{\text{th}} < \mu_{\mathcal{I}}$

For this case, using the results in (92) and (94) and the symmetry of the Gaussian PDF, i.e., the integral equality $\int_{-\infty}^a \frac{1}{\sqrt{2\pi}} e^{-\frac{t^2}{2}} dt \stackrel{a \leq 0}{=} \int_{-a}^{\infty} \frac{1}{\sqrt{2\pi}} e^{-\frac{t^2}{2}} dt$, it is straightforward to obtain

$$\phi_{\mathcal{I}}(I_{\text{th}}) \stackrel{I_{\text{th}} \leq \mu_{\mathcal{I}}}{=} 1 - \frac{1}{\pi} \int_0^{\frac{\pi}{2}} \exp\left(-\frac{\tilde{I}_{\text{th}}^2}{2 \sin^2 \theta}\right) d\theta, \quad (95)$$

and

$$\varphi_{\mathcal{I}}(I_{\text{th}}) \stackrel{I_{\text{th}} \leq \mu_{\mathcal{I}}}{=} 1 - \frac{2}{\pi} \int_0^{\frac{\pi}{2}} \exp\left(-\frac{\tilde{I}_{\text{th}}^2}{2 \sin^2 \theta}\right) d\theta + \frac{1}{\pi} \int_0^{\frac{\pi}{4} + \frac{\arcsin(\rho)}{2}} \exp\left(-\frac{\tilde{I}_{\text{th}}^2}{2 \sin^2 \theta}\right) d\theta. \quad (96)$$

We obtain (52) by substituting (95) and (96) into (25). Similarly, we get (53) easily by plugging $F_{\mathcal{I}}(I_{\text{th}})$ and (52) into (31).

REFERENCES

- [1] G. J. Foschini and M. J. Gans, "On limits of wireless communications in a fading environment when using multiple antennas," *Wireless Personal Commun.*, vol. 6, pp. 311–335, 1998.
- [2] Í. E. Telatar, "Capacity of multi-antenna Gaussian channels," *European Trans. Telecommun.*, vol. 10, pp. 585–595, 1999.
- [3] D. W. Bliss, A. M. Chan, and N. B. Chang, "MIMO wireless communication channel phenomenology," *IEEE Trans. Antennas Propagat.*, vol. 52, pp. 2073–2082, Aug. 2004.
- [4] M. T. Ivrlač, W. Utschick, and J. A. Nossek, "Fading correlations in wireless MIMO communication systems," *IEEE J. Select. Areas Commun.*, vol. 21, pp. 819–828, June 2004.
- [5] J. Maurer, C. Waldschmidt, T. Kayser, and W. Wiesbeck, "Characterisation of the time-dependent urban MIMO channel in FDD communication systems," in *Proc. IEEE Veh. Technol. Conf.*, Jeju, Korea, 2003, pp. 544–548.
- [6] G. Lebrun, J. Gao, and M. Faulkner, "MIMO transmission over a time-varying channel using SVD," *IEEE Trans. Wireless Commun.*, vol. 4, pp. 757–764, Mar. 2005.
- [7] H. Sampath, P. Stoica, and A. Paulraj, "Generalized linear precoder and decoder design for MIMO channels using the weighted MMSE criterion," *IEEE Trans. Commun.*, vol. 49, pp. 2198–2206, Dec. 2001.
- [8] S. K. Jayaweera and H. V. Poor, "Capacity of multiple-antenna systems with both receiver and transmitter channel state information," *IEEE Trans. Inform. Theory*, vol. 49, pp. 2697–2709, Oct. 2003.

- [9] D. Tse and P. Viswanath, *Fundamentals of Wireless Communication*. Cambridge, UK: Cambridge University Press, 2005.
- [10] W. C. Jakes, Ed., *Microwave Mobile Communications*. New York: IEEE Press, 1994.
- [11] A. Abdi, K. Wills, H. A. Barger, M. S. Alouini, and M. Kaveh, "Comparison of the level crossing rate and average fade duration of Rayleigh, Rice, and Nakagami fading models with mobile channel data," in *Proc. IEEE Veh. Technol. Conf.*, Boston, MA, 2000, pp. 1850–1857.
- [12] N. Youssef, T. Munakata, and M. Takeda, "Fade statistics in Nakagami fading environments," in *Proc. IEEE Int. Symp. Spread Spec. Tech. App.*, Mainz, Germany, 1996, pp. 1244–1247.
- [13] A. Abdi, J. A. Barger, and M. Kaveh, "A parametric model for the distribution of the angle of arrival and the associated correlation function and power spectrum at the mobile station," *IEEE Trans. Veh. Technol.*, vol. 51, pp. 425–434, May 2002.
- [14] A. Abdi, W. C. Lau, M. S. Alouini, and M. Kaveh, "A new simple model for land mobile satellite channels: First- and second-order statistics," *IEEE Trans. Wireless Commun.*, vol. 2, pp. 519–528, May 2003.
- [15] L. H. Ozarow, S. Shamai, and A. D. Wyner, "Information theoretic considerations for cellular mobile radio," *IEEE Trans. Veh. Technol.*, vol. 43, pp. 359–378, May 1994.
- [16] B. M. Hochwald, T. L. Marzetta, and V. Tarokh, "Multiple-antenna channel hardening and its implications for rate feedback and scheduling," *IEEE Trans. Inform. Theory*, vol. 50, pp. 1893–1909, 2004.
- [17] Z. Wang and G. B. Giannakis, "Outage mutual information of space-time MIMO channels," *IEEE Trans. Inform. Theory*, vol. 50, pp. 657–662, Apr. 2004.
- [18] P. Smith and M. Shafi, "An approximate capacity distribution for MIMO systems," *IEEE Trans. Commun.*, vol. 52, pp. 887–890, June 2004.
- [19] S. Wang and A. Abdi, "On the second-order statistics of the instantaneous mutual information of time-varying fading channels," in *Proc. IEEE Int. Workshop Signal Processing Advances in Wireless Communications*, New York, 2005, pp. 405–409.
- [20] —, "On the second-order statistics of the instantaneous mutual information in Rayleigh fading channels," *submitted to IEEE Trans. Inform. Theory*, Dec. 2005. [Online]. Available: <http://arxiv.org/abs/cs.IT/0603027>
- [21] A. Giorgetti, M. Chiani, M. Shafi, and P. J. Smith, "Level crossing rates and MIMO capacity fades: impacts of spatial/temporal channel correlation," in *Proc. IEEE Int. Conf. Commun.*, Anchorage, AK, 2003, pp. 3046–3050.
- [22] N. Zhang and B. Vojcic, "Evaluating the temporal correlation of MIMO channel capacities," in *Proc. IEEE Global Telecommun. Conf.*, St. Louis, MO, 2005, pp. 2817–2821.
- [23] S. Wang and A. Abdi, "Joint singular value distribution of two correlated rectangular complex Gaussian matrices and its application," *submitted to SIAM J. Matrix Anal. Appl.*, Feb. 2006. [Online]. Available: <http://arxiv.org/abs/math.PR/0603170>
- [24] I. S. Gradshteyn, I. M. Ryzhik, and A. Jeffrey, Eds., *Table of Integrals, Series, and Products*, 5th ed. San Diego, CA: Academic, 1994.
- [25] M. K. Simon, *Probability Distributions Involving Gaussian Random Variables: A Handbook for Engineers and Scientists*. Boston, MA: Kluwer, 2002.
- [26] M. K. Simon and M.-S. Alouini, *Digital Communication over Fading Channels*, 2nd ed. New York: Wiley-IEEE Press, 2004.
- [27] S. Wang, "Envelope correlation coefficient for logarithmic diversity receivers revisited," *submitted to IEEE Trans. Commun.*, Feb. 2006.
- [28] W. B. Davenport and W. L. Root, *An Introduction to the Theory of Random Signals and Noise*. New York: Wiley, 1987.
- [29] B. Kedem, *Time Series Analysis by Higher Order Crossings*. New York: IEEE Press, 1994.
- [30] A. T. James, "Distributions of matrix variates and latent roots derived from normal samples," *Ann. Math. Statist.*, vol. 35, pp. 475–501, June 1964.
- [31] K. Acolatse and A. Abdi, "Efficient simulation of space-time correlated MIMO mobile fading channels," in *Proc. IEEE Veh. Technol. Conf.*, Orlando, FL, 2003, pp. 652–656.
- [32] P. Beckmann, *Orthogonal Polynomials for Engineers and Physicists*. Boulder, CO: Golem Press, 1973.
- [33] N. R. Goodman, "The distribution of the determinant of a complex Wishart distributed matrix," *Ann. Math. Statist.*, vol. 34, pp. 178–180, Mar. 1963.
- [34] R. L. Graham, D. E. Knuth, and O. Patashnik, Eds., *Concrete Mathematics: A Foundation for Computer Science*, 2nd ed. Boston, MA: Addison-Wesley, 1994.
- [35] A. K. Gupta and D. K. Nagar, *Matrix Variate Distributions*. New York: Chapman & Hall/CRC, 1999.

[36] А. П. Прудников, Ю. А. Брычков, and О. И. Маричев, Интегралы и ряды. Специальные функции., 1st ed. МОСКВА: ФИМАТЛИТ, 1983.

TABLE I
TAYLOR EXPANSION OF (46) AND THE MAXIMUM DIFFERENCE BETWEEN
(43) AND (46) FOR DIFFERENT (M, N) 'S

(M, N)	Taylor Series of (46)	$\max_{0 \leq \varrho_i \leq 1} (43) - (46) ^\ddagger$
(1, 1)	$0.608\varrho_i^2 + 0.152\varrho_i^4 + \mathcal{O}(\varrho_i^6)$	0.160
(2, 2)	$0.437\varrho_i^2 + 0.218\varrho_i^4 + \mathcal{O}(\varrho_i^6)$	0.230
(3, 3)	$0.372\varrho_i^2 + 0.186\varrho_i^4 + \mathcal{O}(\varrho_i^6)$	0.274
(4, 4)	$0.337\varrho_i^2 + 0.168\varrho_i^4 + \mathcal{O}(\varrho_i^6)$	0.304
(4, 8)	$0.725\varrho_i^2 + 0.178\varrho_i^4 + \mathcal{O}(\varrho_i^6)$	0.085
\vdots	\vdots	\vdots
(4, 12)	$0.824\varrho_i^2 + 0.135\varrho_i^4 + \mathcal{O}(\varrho_i^6)$	0.050
\vdots	\vdots	\vdots
(4, 16)	$0.870\varrho_i^2 + 0.107\varrho_i^4 + \mathcal{O}(\varrho_i^6)$	0.036

\ddagger The maximum difference is calculated via the function FindMaximum in Mathematica®.

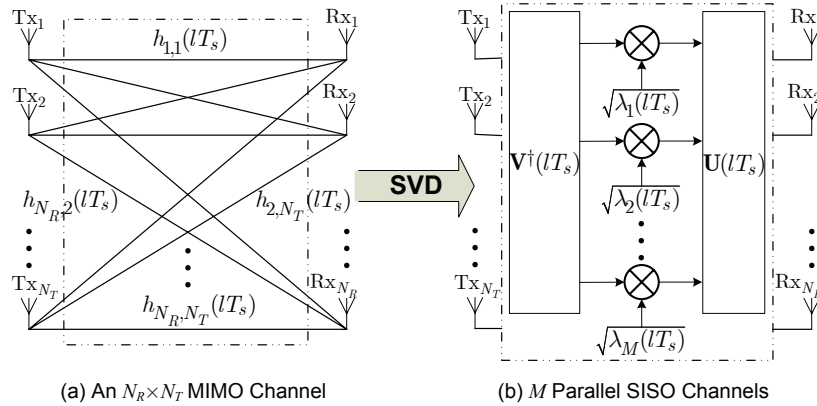


Fig. 1. (a) A MIMO channel with N_T transmit and N_R receive antennas; (b) The equivalent M parallel SISO channel representation.

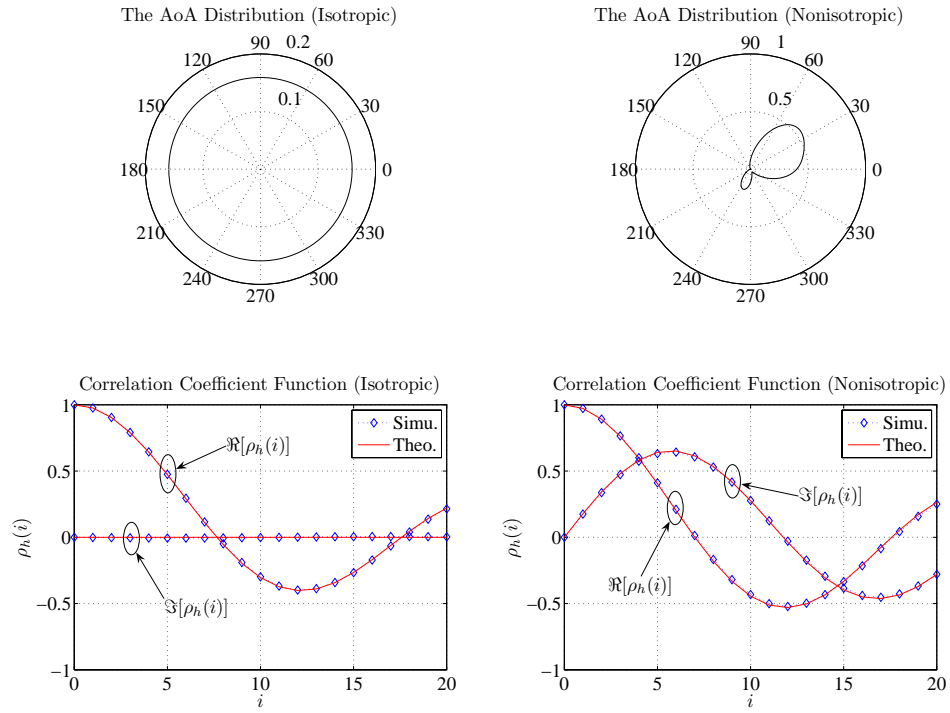


Fig. 2. The AoA distributions for two scattering examples and the corresponding channel correlation coefficients.

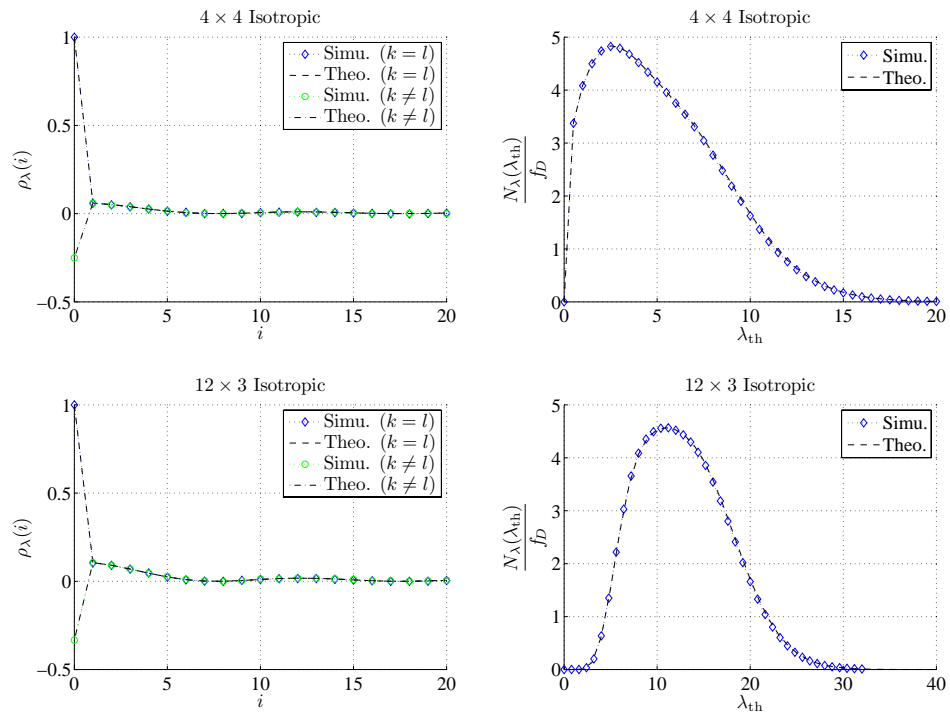


Fig. 3. The correlation coefficient and the LCR of an *eigen-channel*, in 4 × 4 and 12 × 3 MIMO systems with *isotropic* scattering.

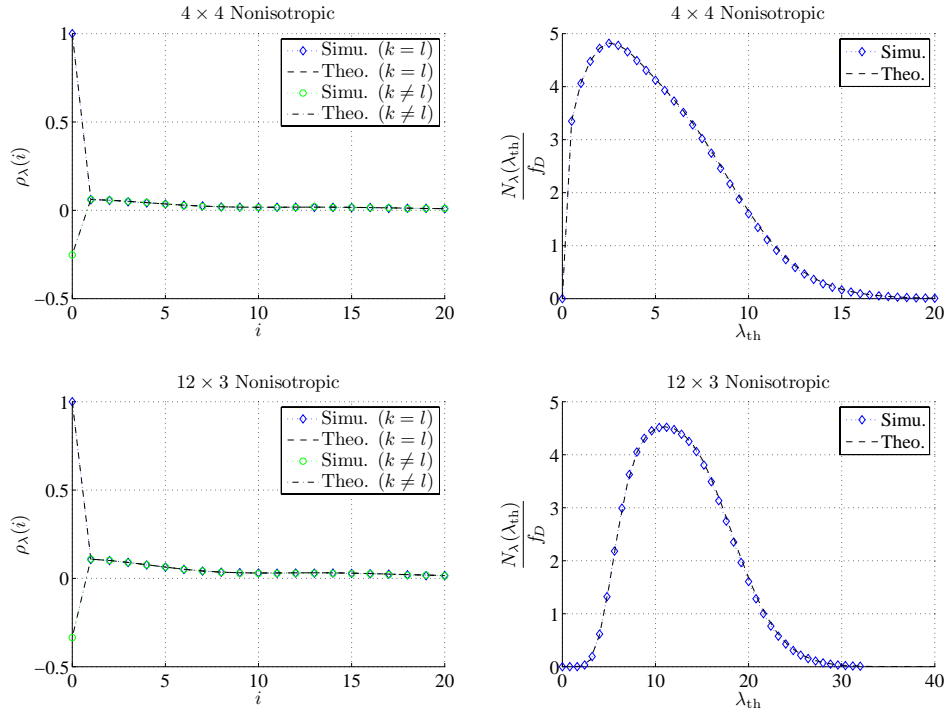


Fig. 4. The correlation coefficient and the LCR of an *eigen-channel*, in 4×4 and 12×3 MIMO systems with *nonisotropic* scattering.

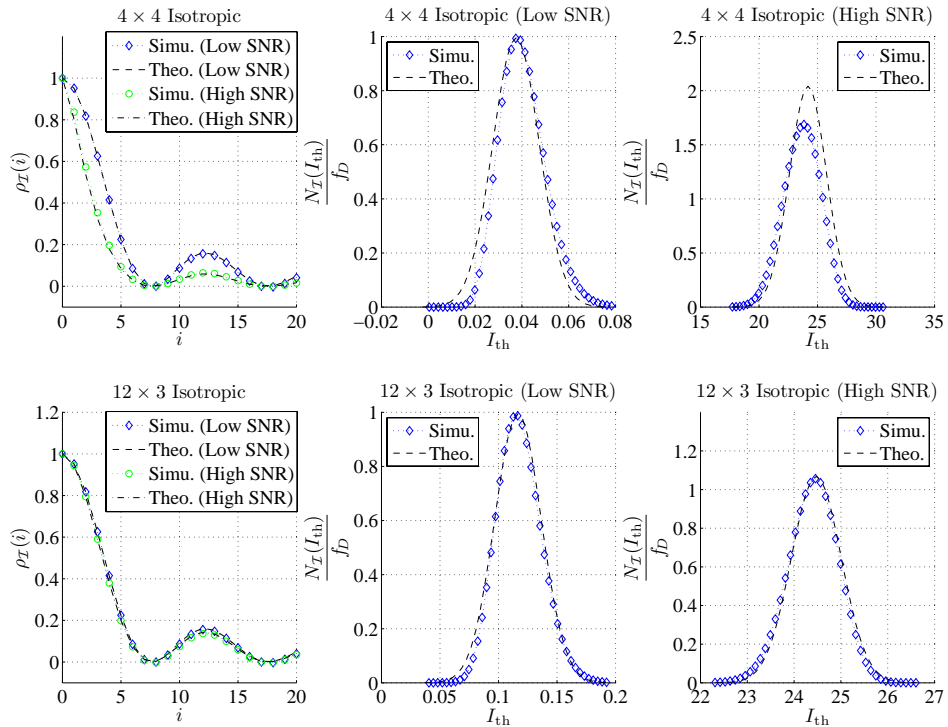


Fig. 5. The correlation coefficient and the LCR of the MIMO IMI at low- and high-SNR regimes, in 4×4 and 12×3 MIMO systems with *isotropic* scattering.

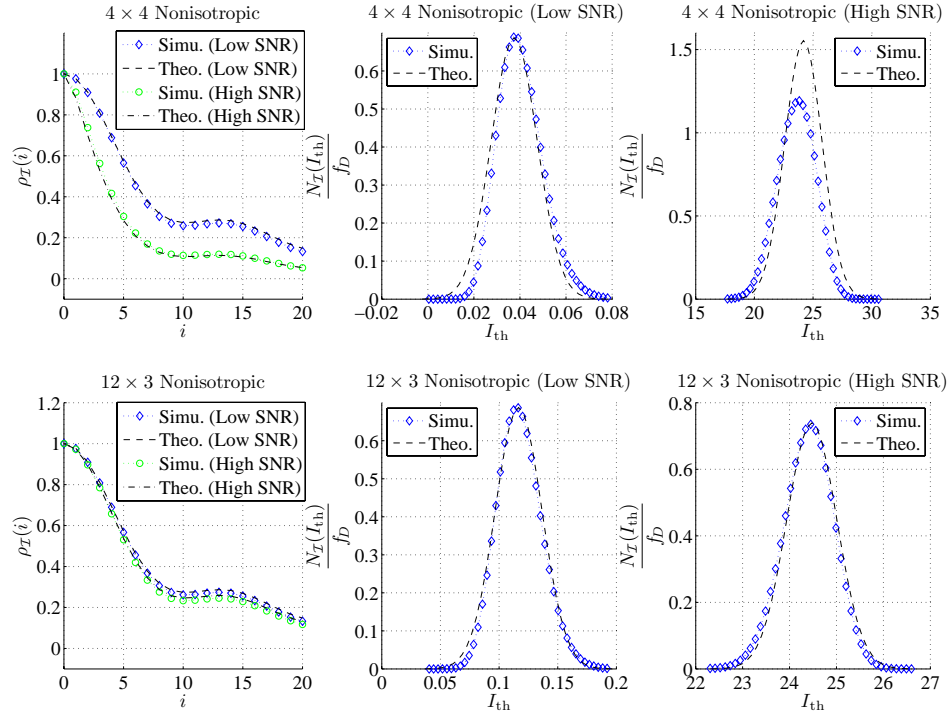


Fig. 6. The correlation coefficient and the LCR of the MIMO IMI at low- and high-SNR regimes, in 4×4 and 12×3 MIMO systems with *nonisotropic* scattering.

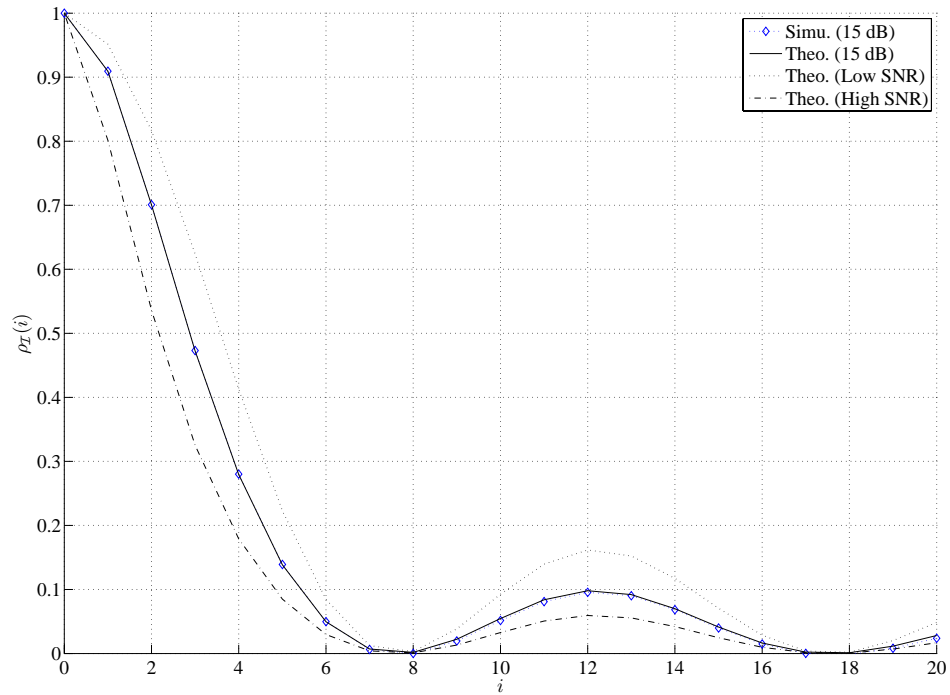


Fig. 7. The correlation coefficient of the MIMO IMI at $\eta = 15$ dB (moderate SNR), in a 4×4 system with *isotropic* scattering.